# Phase separation in vacuum codeposited pentacene/6,13-pentacenequinone thin films

Ingo Salzmann, Ricarda Opitz, Siegfried Rogaschewski, Jürgen P. Rabe, and Norbert Koch*
*Institut für Physik, Humboldt-Universität zu Berlin, Newtonstraße 15, D-12489 Berlin, Germany*

Bert Nickel
*Department für Physik and CeNS, Ludwig-Maximilians-Universität, Geschwister-Scholl-Platz 1, D-80539 München, Germany*
(Received 11 September 2006; revised manuscript received 25 January 2007; published 16 May 2007)

Pentacene (P) and 6,13-pentacenequinone (PQ) have been vacuum codeposited onto $SiO_2$ in order to control phase separation in thin films for the application as bulk heterojunctions in organic photovoltaic devices. Structural investigations by means of scanning electron microscopy (SEM) and atomic force microscopy revealed pronounced phase separation of the two materials at length scales that turned out to be tunable by the variation of the deposition rate. X-ray diffraction provided evidence for polymorphism in pure films of P and PQ on $SiO_2$. While pure films exhibited both the bulk and thin-film phase, the bulk phase is mainly suppressed within the co-deposited films (P+PQ). This was corroborated by Fourier-transform infrared spectroscopy results. SEM investigations of pure and codeposited films indicated that PQ bulk crystallites of up to 200 nm height form continuous paths to the substrate and grow within a matrix formed of P and PQ thin-film phases. The obtained heterojunction morphologies thus appear interesting for the application in organic-based photovoltaic cells.

DOI: 10.1103/PhysRevB.75.174108 PACS number(s): 61.66.Hq, 68.55.−a, 68.37.−d, 61.10.Nz

## I. INTRODUCTION

Crystals of conjugated organic molecules are regarded as interesting for a large variety of electronic and optoelectronic applications and their structural and electronic properties have been widely investigated throughout the last years.[1–8] Pentacene (P) is a prototypical material in the field of organic electronics due to its high charge-carrier mobility of up to 5.5 $cm^2/V$ s in organic thin-film transistors.[9–13] Considerable effort has been made to investigate the structure of P thin films, since the intermolecular arrangement governs the highly anisotropic transport properties of oligoacenes.[14] In addition, chemical impurities in P films and crystals were identified to have a tremendous impact on the charge-carrier mobility. For instance, the presence of 6,13-pentacenequinone (PQ) ($C_{22}H_{12}O_2$) leads to a significant reduction of charge-carrier mobility in P single crystals at concentrations as low as 0.68%.[15] In addition, it was suggested that PQ can form deep traps for electrons within a P matrix, with depths ranging from 0.2 to 0.75 eV, depending on the mutual molecular orientation.[16] This may explain, to some extent, why the electron mobility reported for pentacene is notoriously lower than that of holes.[17–20] However, no information is available on the impact of the presence of PQ on the resulting structure and morphology of P thin films. Even slight changes in intermolecular arrangements can lead to a number of shallow traps in thin films causing inferior charge-carrier mobilities.[21]

The intrinsic electronic properties of sequentially deposited P and PQ thin films on $SiO_2$ have been investigated in recent ultraviolet photoelectron spectroscopy studies, which revealed an energy-level offset between the highest occupied molecular orbital levels of 1.4 eV.[16] Together with the values found for the respective optical band gaps of 1.8 eV (P) and 2.8 eV (PQ) (Sec. V) and the value of the pentacene electron affinity of ~2.7 eV,[22] the estimated energy-level arrangement appears suitable for the use in bulk-heterojunction photovoltaic devices produced by codeposition.[23–27] The morphology as well as the structural properties of codeposited films are herein decisive in order to evaluate the applicability as interpenetrating donor/acceptor network within this field of application.

The investigation of the structural properties of thin films composed of P and PQ is also of particular interest from a more fundamental viewpoint: While both molecules have similar length and are rigid and planar, the crystal structures of pure P and PQ differ significantly. Several polymorphs have been observed for P, which can be distinguished by the spacing of the (001) cleavage planes, ranging from 1.41 to 1.44 nm for P single crystals (bulk phase) and 1.54 nm for thin films thermally evaporated on $SiO_2$ substrates (thin-film phase).[14,28–32] The molecules form a layered structure perpendicular to this plane and adopt a herringbone arrangement within such a plane. The PQ single-crystal structure also exhibits a comparable layered structure along the (020) cleavage planes, however, with a smaller spacing of 0.89 nm.[33] For PQ, the molecular planes are parallel within the layers, i.e., no internal herringbone structure exists. However, the long molecular axes and planes of molecules in neighboring layers are tilted with respect to each other. It is therefore important to know whether P and PQ—somewhat similar on a molecular level but largely different in their crystal structure—form a mixed crystal (intercalationlike) or whether phase separation prevails if both compounds are simultaneously present during the crystallization process. This question is addressed in the present study by investigating the morphology and structure of P and PQ thin films prepared by codeposition.

## II. EXPERIMENT

Pentacene and 6,13-pentacenequinone (purchased from Aldrich and used without further purification) thin films were

 ©2007 The American Physical Society

obtained by vacuum deposition (base pressure of $3 \times 10^{-7}$ mbar) from a ceramic crucible that was resistively heated. The nominal film thickness ($\chi$) was measured *in situ* by a quartz microbalance. Substrates were (100) *p*-doped silicon wafers (Siegert Consulting, prime grade) with a thermally grown oxide layer of 50 nm, cut into $10 \times 10$ mm$^2$ coupons. The root-mean-square roughness of the $SiO_2$ substrates was 0.15 nm as determined by atomic force microscopy (AFM). These substrates were used as received, and their cleanliness was confirmed by AFM investigations prior to organic film deposition. Two side polished fused silica (quartz) substrates (Präzisions Glas & Optic GmbH) were used for optical-absorption experiments. Prior to organic material deposition, they were cleaned by sonication subsequently in acetone, isopropanol (both at 50 °C), and deionized water.

Optical-absorption measurements were performed using a Shimadzu UV-2101PC spectrometer at a resolution of 1 nm. X-ray-diffraction measurements were performed at the beamline W1.1 at the synchrotron radiation source HASYLAB (Hamburg, Germany). For x-ray-diffraction texture analysis, a Philips MRD four-circle goniometer with a Cu $K\alpha$ tube was used. Fourier-transform infrared (FTIR) absorption spectroscopy measurements (resolution of 2.8 cm$^{-1}$, near-normal transmission geometry) were performed with a Bruker IFS-66v spectrometer using a midrange mercury cadmium telluride detector cooled with liquid nitrogen. Scanning electron microscopy (SEM) investigations were carried out with a Cambridge Instruments S360 scanning electron microscope. In order to avoid charging problems during SEM measurements, organic thin-film samples were coated with a 3 nm Au film. AFM investigations were performed with a Veeco Nanoscope III in TappingMode. Step heights ($h$) were analyzed by means of elevation histograms of AFM micrographs considering areas of at least $5 \times 5$ $\mu$m$^2$.

## III. RESULTS: MORPHOLOGY

### A. Thin PQ films

In contrast to the case of P, where extensive growth studies have already been carried out for submonolayer[32,34–39] and for multilayer films,[5,28] no systematic investigation on PQ thin-film growth has been reported yet.

We analyzed thin films of PQ on $SiO_2$ (deposition rate $\kappa$=0.1 nm/min) by means of AFM at various film thicknesses, and representative results for a nominal submonolayer film ($\chi$=0.8 nm) and a film in the multilayer range ($\chi$=3.2 nm) are shown in Figs. 1(a) and 1(b) and respectively. In both cases, we found pronounced island growth of Volmer-Weber type, as no indication for the presence of a wetting layer could be found. This is in contrast to the Stranski-Krastanov-type growth reported for P thin films on $SiO_2$, where at least one complete layer is being formed on which island are built up.[40] The PQ submonolayer film exhibits an area coverage of only 10% (due to the instant formation of multilayer islands) and an island density ($N$) of 1.4 $\mu$m$^{-2}$. For comparison, a P film of same nominal thickness had a coverage of 50% and $N$=5.5 $\mu$m$^{-2}$. These values

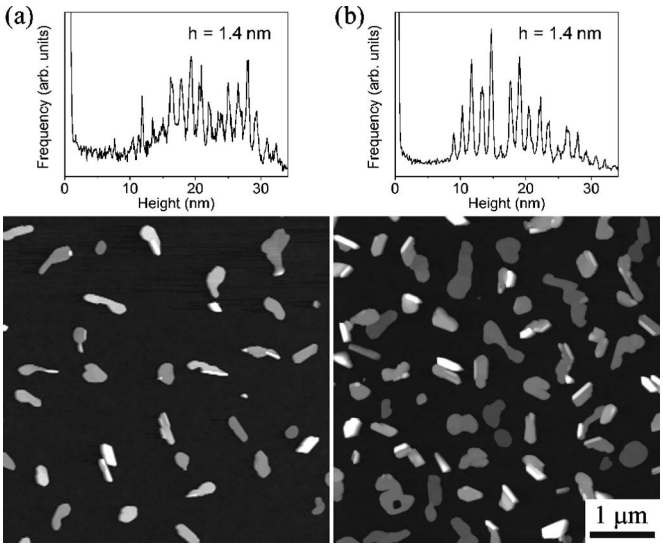


FIG. 1. AFM height images of PQ films of (a) $\chi$=0.8 nm [coverage 10%, island density ($N$)=1.4 $\mu$m$^{-2}$] and (b) $\chi$=3.2 nm (coverage 30%, $N$=2.3 $\mu$m$^{-2}$) on $SiO_2$ ($\kappa$=0.1 nm/min) together with the corresponding elevation histograms showing stepped terraces of height $h$.

are increased to 30% coverage and $N$=2.3 $\mu$m$^{-2}$ for the PQ film of nominally 4 monolayer thickness ($\chi$=3.2 nm). The pronounced island growth indicates that PQ molecules have a large diffusion constant on the $SiO_2$ surface and that the growth is dominated by intermolecular interaction of PQ molecules as opposed to the interaction between the molecules and the substrate. The AFM micrographs reveal the presence of two different kinds of island morphologies: (1) smooth, plane islands with comparable dimensions within the substrate plane (mean height ~15 nm) that show pronounced internal steps, as well as (2) needlelike crystallites of up to 100 nm height without detectable internal steps. From the corresponding elevation histograms the internal step heights of the islands of type (1) were determined to be $h$=1.4±0.2 nm. Note that this step height agrees with the reported value of 1.27 nm found for the interplanar spacing of the (001) net planes within a thin-film phase of PQ by x-ray diffraction (XRD).[41] As will become apparent from additional studies presented below, we attribute the two distinctly different morphologies to two coexisting different PQ polymorphs, i.e., the bulk phase and a substrate-induced thin-film phase (see Sec. IV).

### B. Thin P+PQ films

In order to investigate the early stage of the growth of P+PQ codeposited films (ratio P:PQ=1:1) on $SiO_2$, samples of $\chi$=1.6 nm were prepared at two different deposition rates, i.e., $\kappa$ of total 0.1 nm/min [Fig. 2(a)] and 6 nm/min [Fig. 2(b)], and investigated by means of AFM. In the case of low $\kappa$, we can distinguish two types of morphologies: Approximately 50% of the substrate is covered by flat islands of 1.8±0.4 nm height, which closely resemble the morphology of thin films of P only [see Fig. 4(a)]. This step height is comparable to the reported values of 1.54 nm (Refs. 30, 34,

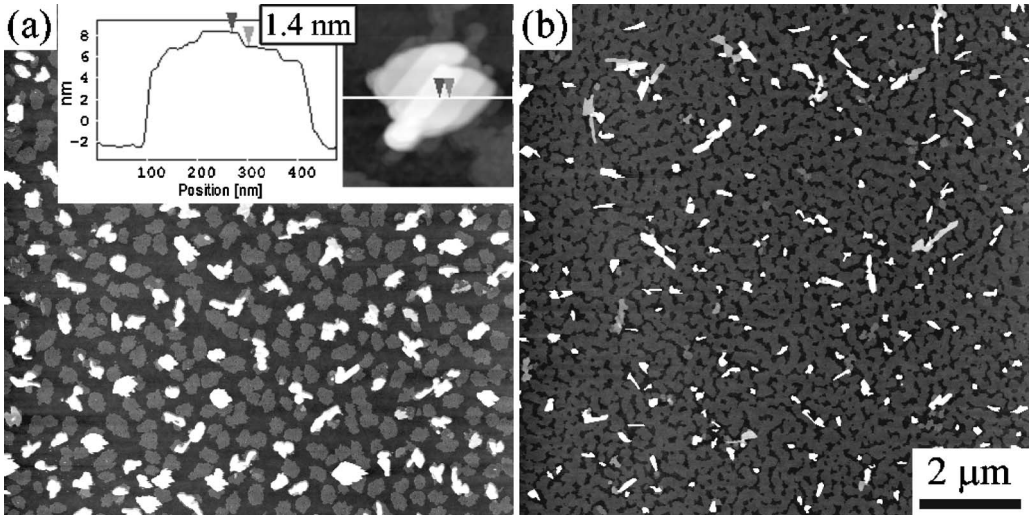


FIG. 2. AFM height images of 1:1 codeposited P+PQ films of total $\chi$=1.6 nm deposited at rates of total (a) 0.1 nm/min and (b) 6 nm/min on $SiO_2$. The inset in (a) shows a zoomed view of a typical island assigned to PQ exhibiting terraces with a step height of ~1.4 nm.

38, 42, and 43) for the (001) lattice spacing of the P thin-film phase and 1.61 nm (Ref. 32) for the P monolayer thickness.[65]

In addition, ~13% of the surface is covered by islands of average total height of ~10 nm with internal steps and somewhat different shape [$N$=1.7 $\mu m^{-2}$, see inset in Fig. 2(a)]. They are assigned to PQ due to their similarity to films of pure PQ (Fig. 1). The step heights were determined from the corresponding AFM height histograms (Fig. 3). For higher deposition rates of 6 nm/min, we found an increased density of P monolayer islands, as expected by previous work.[44] The same effect was observed for the islands assigned to PQ (coverage 8%, $N$=3.2 $\mu m^{-2}$), which exhibit an average island height that is nearly doubled to 17 nm (compared to 10 nm for the film prepared with $\kappa$=0.1 nm/min).

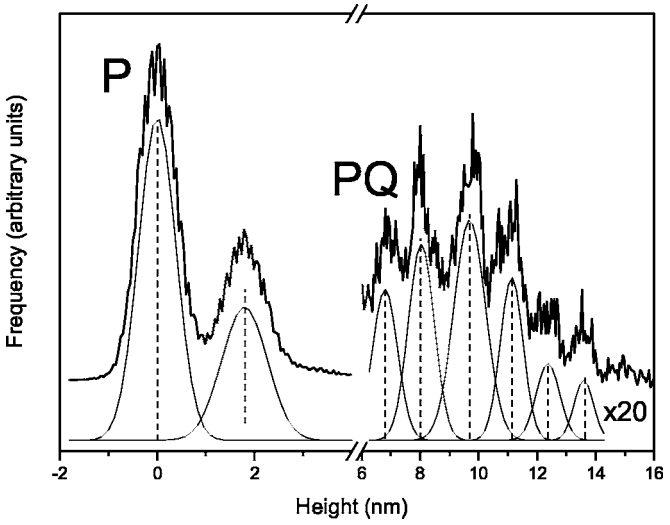


FIG. 3. Elevation histogram of the AFM height image in Fig. 2(a) together with Gaussian fits. The peak at the origin represents the substrate level; at a mean step height of 1.8±0.4 nm contributions from the P monolayer can be found. Steps of 1.4±0.2 nm at elevated heights result from PQ multilayers.

The intrinsic PQ step height was identical to the low-$\kappa$ sample. In addition, a higher $\kappa$ apparently leads to an increase of the relative amount of the islands that exhibit the characteristic PQ steps. From our AFM investigations in the submonolayer range of codeposited thin films, we obtain indications for pronounced phase separation of P and PQ, which is substantiated in the following sections.

### C. Sequential deposition

The results of the previous section pose the question whether P and PQ islands grow next to or on top of each other. This issue was addressed through sequential deposition of the two materials. Growth parameters were adjusted in order to achieve equal island densities of the P ($\kappa$ =1 nm/min) and PQ ($\kappa$=6 nm/min) underlayers [Figs. 4(a) and 4(c)]. In both cases of sequential deposition (PQ on P [Fig. 4(b)] and P on PQ [Fig. 4(d)]), the later evaporated compound was apparently found to be growing on top of the first. In addition, the respective islands of both materials adopt the shape of the underlying layer. The characteristic step heights found in both layered samples are in agreement with the values found for codeposited films (Fig. 2). Note that the island coalescence for overlayer PQ on P is more pronounced than for the reverse case. This is in contrast to the morphology found for codeposited samples, and may thus indicate that PQ islands in Fig. 2 grow next to islands of P. Interestingly, no evidence for the appearance of the needlelike phase could be found in the case of sequential evaporation of PQ onto a submonolayer of P.

### D. P, PQ, and P+PQ films of $\chi$=30 nm

For devices, the relevant film thicknesses are larger than those presented so far. Therefore, we investigated the morphology and the structure of $\chi$=30 nm thin films of pure P and PQ films ($\kappa$=0.5 nm/min) as well as codeposited samples (P:PQ ratio of 1:1, total $\kappa$=0.5 and 6 nm/min) on

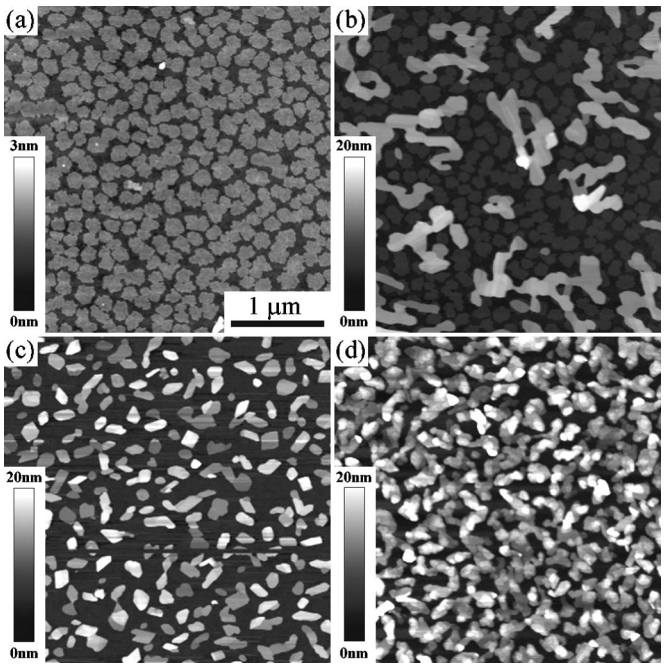


FIG. 4. AFM height images of layered thin films of P and PQ on $SiO_2$ for different $\kappa$ and comparable island densities. (a) shows a P film of $\chi=1$ nm ($\kappa=1$ nm/min) and (b) a 2-nm-thick PQ film ($\kappa=0.1$ nm/min) on top. (c) shows the underlayer film of 3.2 nm PQ ($\kappa=6$ nm/min) for a P film of $\chi=1$ nm (0.1 nm/min) (d). The sequential deposition processes were performed immediately in succession without breaking the vacuum.

$SiO_2$ by means of AFM, x-ray diffraction, and FTIR. For pure P films ("sample P"), the AFM micrograph in Fig. 5(a) shows the well-known stepped terracelike morphology of the thin-film phase[5,28,35,36,45] with typical steps of $h=1.6\pm0.2$ nm, which were obtained via AFM step height analysis during different stages of the growth process [inset in Fig. 5(a)]. For the pure PQ film ["sample PQ," Fig. 5(b)], we find a total coverage of only 65% of the substrate surface despite the nominal film thickness of about 20 monolayers. This observation of incomplete $SiO_2$ coverage by PQ agrees with the findings presented for the $\chi=0.8$ and 3.2 nm films (Fig. 1). Again, a two phase morphology is apparent, which consists of both the planar phase (1) areas and elevated needlelike structures of phase (2) (here up to 200 nm high), as already found for the thin PQ films (Fig. 1). Analogously, we assign the two morphologies to areas grown in the thin film and in bulk phase, respectively. The analysis of the elevation histogram [inset in Fig. 5(b)] yields a frequency maximum for island heights of ~40 nm (PQ thin-film phase) covering 40% of the substrate. By integrating the respective areas of the histogram, we can estimate the volume ratio between the two phases to be 1:1. The morphology of the codeposited film ["sample P+PQ," Fig. 5(c)] shows areas of granular structure (height range <20 nm) together with islands of needlelike shape (heights up to 200 nm). From a comparison to our results for the morphology of pure P films [Fig. 5(a)], pure PQ films [Figs. 1 and 5(b)], as well as P+PQ films (Fig. 2), we assign the islands marked in Fig. 5(d) to islands of the PQ bulk phase, the planar islands marked in

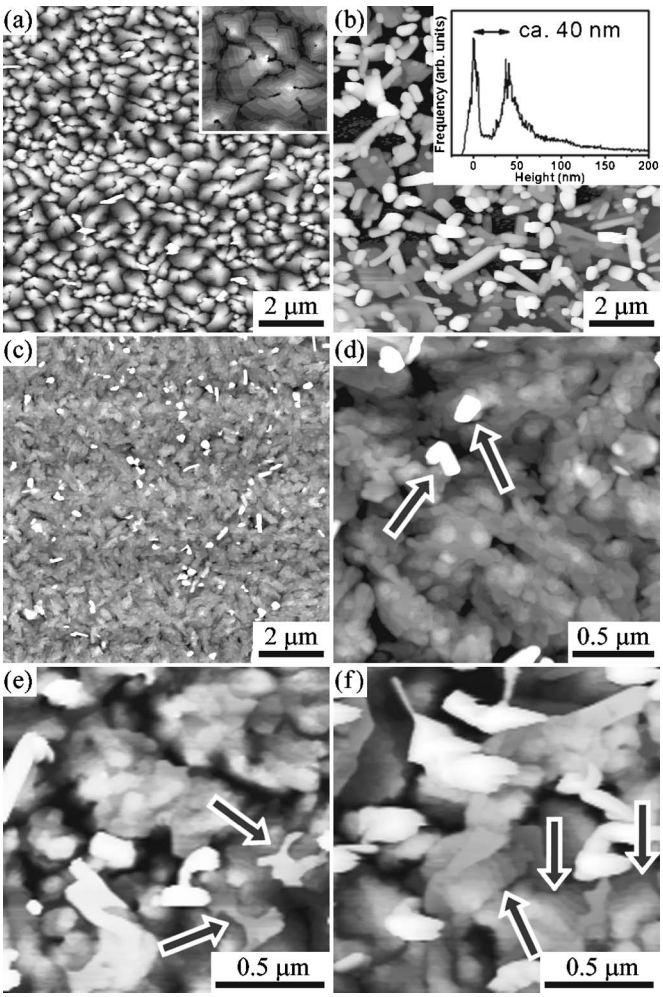


FIG. 5. AFM height image of samples (a) P, (b) PQ, and (c) P+PQ ($\kappa=0.5$ nm/min) on $SiO_2$ together with zoomed representations [(d)–(f)]. The inset in (a) shows a $2.5\times2.5$ $\mu m^2$ image of intermediate $\chi$ of 5 nm, while the inset in (b) shows the elevation histogram of the pure PQ film. Arrows in (d)–(f) point to islands assigned to the (d) PQ-bulk phase, (e) the PQ thin-film phase, and (f) the P thin-film phase (see text).

Fig. 5(e) to islands of the PQ thin-film phase, and the stepped structures showing again steps of $h=1.6\pm0.2$ nm in Fig. 5(f) to P thin-film phase islands. For the pure PQ film, we find 15% of the surface area covered by the PQ bulk, whereas this amount reduces to 8% in the case of P+PQ films. This indicates that the process of codeposition of the two materials leads to preferred growth of PQ within the thin-film phase.

In order to obtain more information on the vertical composition of the P+PQ film, we investigated the two P+PQ samples deposited at different $\kappa$ by SEM. For that purpose, samples were broken along a preferential direction of the Si wafer to allow for cross-section viewing along edges. Figures 6(a) and 6(b) show on-top views of different $\kappa$ samples, and images of the cross-section view (for a sample tilt of 80°) are shown in Fig. 6(c). As already inferred from the AFM investigations, the SEM top view supports the notion of pronounced phase separation of P and PQ within the codeposited film. One can clearly distinguish needlelike crystallites, which were assigned to the PQ bulk (at low $\kappa$: 8%

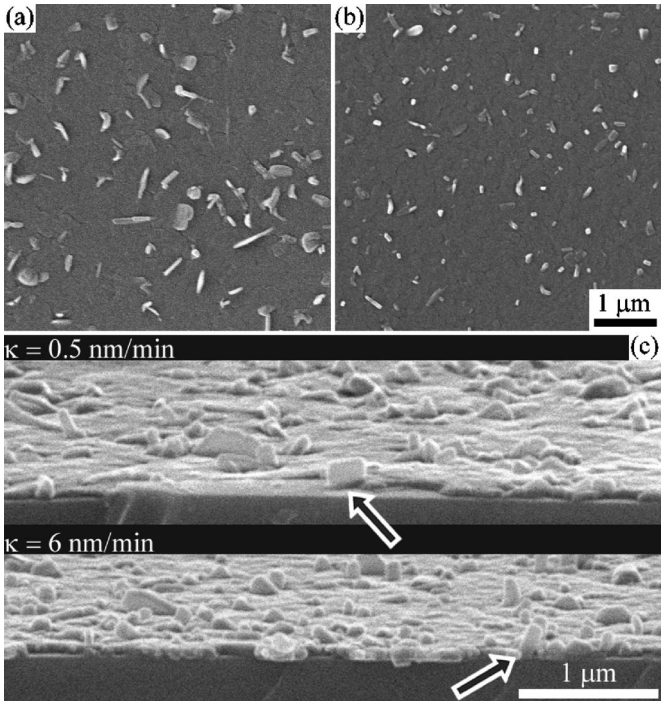


FIG. 6. SEM micrographs of codeposited P+PQ films of 30 nm nominal thickness at different deposition rates $\kappa$ of total (a) 0.5 nm/min and (b) 6 nm/min under top view. The images in (c) show the cut edge of the two samples and were recorded under a sample inclination of 80°.

coverage, island density of 3 $\mu m^{-2}$). These needles seem to be embedded within a closed and rather smooth film (composed of P and PQ thin-film phases, which cannot be distinguished by SEM). From the cross-section view, we can estimate the height of the PQ bulk islands [sample islands marked by arrows in Fig. 6(c)] to be ~200 nm, whereas the thickness of the surrounding P/PQ film matrix is estimated to be ~20 nm. The investigation of several crystallites in the vicinity of the cut edge indicates a direct growth on the substrate within the resolution limits of SEM (~10 nm). The increase of the deposition rate $\kappa$ to 6 nm/min yields a reduced value of 0.8±0.2 $\mu$m for the interisland distance and reduces the area covered by PQ bulk islands by a factor of about 2. In this case, the island density is nearly doubled to 5 $\mu m^{-2}$, which is also apparent in the SEM micrograph shown in Fig. 6(b).

## IV. RESULTS: CRYSTAL STRUCTURE

From our investigation of the thin-film morphologies, we already found strong indications for polymorphism of PQ in both pure and codeposited films, and we proposed growth within a PQ thin film and the bulk phase. In order to pin down this assumption, we performed specular x-ray-diffraction scans on that same set of samples. The pure PQ films of $\chi$=3.2 nm [Fig. 7(a)] and 30 nm [Fig. 7(b)] exhibit indeed polymorphic growth within a thin film and the bulk phase. We found a preferred orientation of the bulk (0$k$0) net planes parallel to the substrate, which is inferred from a comparison of a calculated powder spectrum[46,47] and the experimental one in Fig. 7. Within the film of $\chi$=3.2 nm, we find reflections of the bulk (0$k$0) series up to $k$=6 (reflection condition $k=2n$ due to the monoclinic space group $P2_1/b$) as well as a small contribution of the (021) plane [intensity ratio between (021) and (020) ~1:100]. The thick film of $\chi$ =30 nm shows contributions of the same orientation, and all bulk peak positions were found in perfect agreement with the calculated spectrum of the PQ bulk (experimental values are listed in Table I). The orientation of PQ molecules with respect to the plane (020) is illustrated in Fig. 8 (viewed along the axes of the unit cell) and we can identify the plane as a cleavage plane of the crystal. The reflection found at the lowest momentum transfer (marked with a circle in Fig. 7) corresponds to the lattice spacing ($d_{hkl}$) of $d_{001}$ of 1.305 nm for (001) planes of the PQ thin-film phase, which we already proposed from the step height analysis from the AFM micrographs ($h$=1.4±0.2 nm). Reflections of this orientation are found up to fourth order in the thin, whereas only the first order can be clearly seen in the spectrum of the PQ film of 30 nm nominal thickness. Considering the van der Waals length of a single PQ molecule of 1.61 nm, we estimate that PQ molecules are tilted by ~36° with respect to the substrate surface normal for the thin-film polymorph. Note that our result deviates by 0.035 nm from a previously reported value[41] for the lattice spacing $d_{001}$ of the PQ thin-film phase. For the pure P film ($\chi$=30 nm), we find reflections that can be assigned to the (001) series of the P thin-film phase (square symbols in Fig. 9) with a characteristic $d_{001}$ layer thickness of 1.55 nm (Table I). In addition, two weak contributions of the P bulk structure[30] can be found. Thus, the results obtained from x-ray diffraction nicely support the AFM-based proposal for the polymorphism in pure PQ films.

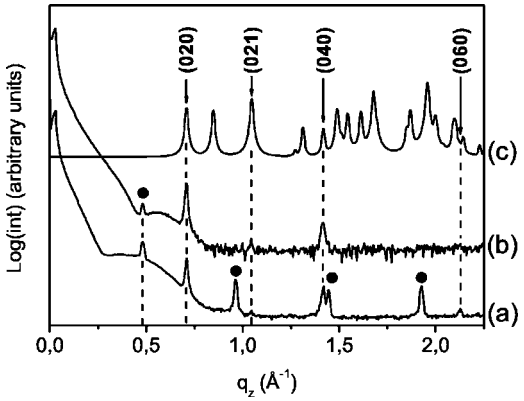


FIG. 7. Specular x-ray-diffraction scan of (a) a 3.2 nm [AFM micrograph in Fig. 1(b)] and (b) a 30 nm [AFM micrograph in Fig. 5(b)] PQ film on $SiO_2$ compared to a calculated PQ powder spectrum (CSD refcode PENTQU) (Ref. 46). Spectrum (c) has been normalized with respect to the experimental (020) reflection intensity of scan (b); (060) is hidden in the shoulders of neighboring peaks.

We now turn toward the codeposited film (low $\kappa$), where we find two series of Bragg peaks, which can be assigned to the respective thin-film phases of P and PQ (Fig. 9, curve P+PQ). However, no significant contributions from the respective bulk phases are observed. In contrast to P, where the

TABLE I. Positions of the Bragg reflections found in the x-ray-diffraction scans shown in Fig. 9. Reflections of planes (*hkl*) of the bulk phases are denoted as P(*hkl*) and PQ(*hkl*), while reflections of the thin-film phases are denoted as TP(*hkl*) for P and TQ(*hkl*) for PQ, respectively. $q_z$ indicates the momentum transfer, $D$ the out-of-plane crystalline coherence length estimated by the Scherrer formula, and $d_{hkl}$ the resulting plane spacing of lattice planes (*hkl*).

| | Pentacene | | | 6,13-pentacenequinone | | | Co-deposited | | |
|---|---|---|---|---|---|---|---|---|---|
| | $q_z$ (Å$^{-1}$) | $D$ (Å) | $d_{hkl}$ (Å) | $q_z$ (Å$^{-1}$) | $D$ (Å) | $d_{hkl}$ (Å) | $q_z$ (Å$^{-1}$) | $D$ (Å) | $d_{hkl}$ (Å) |
| TP(001) | 0.406 | 449 | 15.47 | | | | 0.406 | 494 | 15.48 |
| TQ(001) | | | | 0.482 | 469 | 13.05 | 0.477 | 502 | 13.17 |
| PQ(020) | | | | 0.708 | 323 | 8.87 | | | |
| TP(002) | 0.813 | 446 | 7.73 | | | | 0.815 | 461 | 7.71 |
| TQ(002) | | | | | | | 0.957 | 387 | 6.56 |
| PQ(021) | | | | 1.041 | 103 | 6.04 | | | |
| TP(003) | 1.219 | 444 | 5.15 | | | | 1.220 | 382 | 5.15 |
| P(1-10) | 1.364 | 391 | 4.61 | | | | | | |
| PQ(040) | | | | 1.416 | 274 | 4.44 | | | |
| TQ(003) | | | | | | | 1.434 | 298 | 4.38 |
| TP(004) | 1.626 | 425 | 3.87 | | | | 1.627 | 391 | 3.86 |
| P(022) | 1.696 | 703 | 3.70 | | | | | | |
| TQ(004) | | | | | | | 1.917 | 301 | 3.28 |
| TP(005) | 2.032 | 388 | 3.09 | | | | 2.033 | 328 | 3.09 |

same number of reflections appears as for the pure film (but with reduced intensity), we can now find the peaks of the PQ thin-film phase up to (004). This finding matches our results from morphological investigations, where we found preferred growth of the PQ thin-film phase for codeposition (an increase of ~50% if compared to the pure film).

In more detail, the complete disappearance of the PQ bulk (020) reflection in the specular scan points to a differently or significantly less textured growth of the PQ bulk crystallites in the codeposited film, since PQ bulk crystallites are clearly visible in both AFM and SEM micrographs of the codeposited film. The method of choice to assess this issue is the x-ray-diffraction pole figure (XRD-PF) technique, where the goniometer is fixed to the momentum transfer of a certain $d_{hkl}$ and the plane normal to the sample surface is being tilted with respect to the scattering vector by an angle $\psi$. We performed such experiments. However, for XRD-PF scans in the range $0° < \psi < 85°$ for the (020) and (140) reflections of the PQ bulk (the latter is the most intense peak of the powder spectrum), we found no evidence for the respective Bragg peaks. Therefore, we conclude that the bulk phase needlelike crystallites observed with AFM and SEM do not grow significantly textured in case of codeposition. One can thus think of the bulk crystallites as "powder" of too low scattering intensity to be detected in our experimental setup. Interestingly, the (001) reflection in the spectrum of P+PQ is shifted by $q_z = 0.005$ Å$^{-1}$ compared to the pure film, which corresponds to an increase of $d_{001}$ of the thin-film phase of 0.013 nm. We assign this to strain induced in PQ by the coexistence with P, which hence leads to a slightly reduced inclination of the PQ molecules with respect to the substrate surface in this polymorph. All peak positions of x-ray-diffraction results for films of $\chi = 30$ nm are summarized in Table I. In addition, the out-of-plane crystalline coherence length ($D$) was estimated using the Scherrer formula:[48,49] $D \approx 2\pi/\mathrm{FWHM}\ (q_z)$, where FWHM ($q_z$) are the corresponding full widths at half maximum of the Bragg peaks. The finding that the $D$ values of the P and PQ thin-film phases do not differ significantly for pure ($\chi = 30$ nm) and codeposited films (total $\chi = 30$ nm) is further evidence for pronounced phase separation in the latter. In the case of the codeposited film at elevated $\kappa$ of 6 nm/min [SEM micrograph in Fig. 6(b)], a specular x-ray-diffraction scan yields a significant intensity increase of the PQ thin-film phase (001) reflection in relation to the P thin-film phase (001) reflection (not shown). This supports further the finding from the SEM investigations that an increase of $\kappa$ decreases the amount of PQ within its bulk phase.

## V. RESULTS: VIBRATIONAL AND OPTICAL PROPERTIES

FTIR spectroscopy has already been successfully used in the study of polymorphism of organic molecular crystals.[2,50–53] In contrast to XRD, where only contributions of crystalline domains can be detected, FTIR provides additional information about the entire sample, since also noncrystalline phases contribute to IR absorption. By and large, these could be identified by changes in vibrational energies compared to crystalline phases. Therefore, FTIR is highly sensitive to sample volumes that potentially contain noncrystalline or intercalated P and PQ. Figure 10 shows the absorption spectra of the respective pure and codeposited films on $SiO_2$ compared to reference spectra provided by the manufacturer for the two materials (each corresponding to the re-

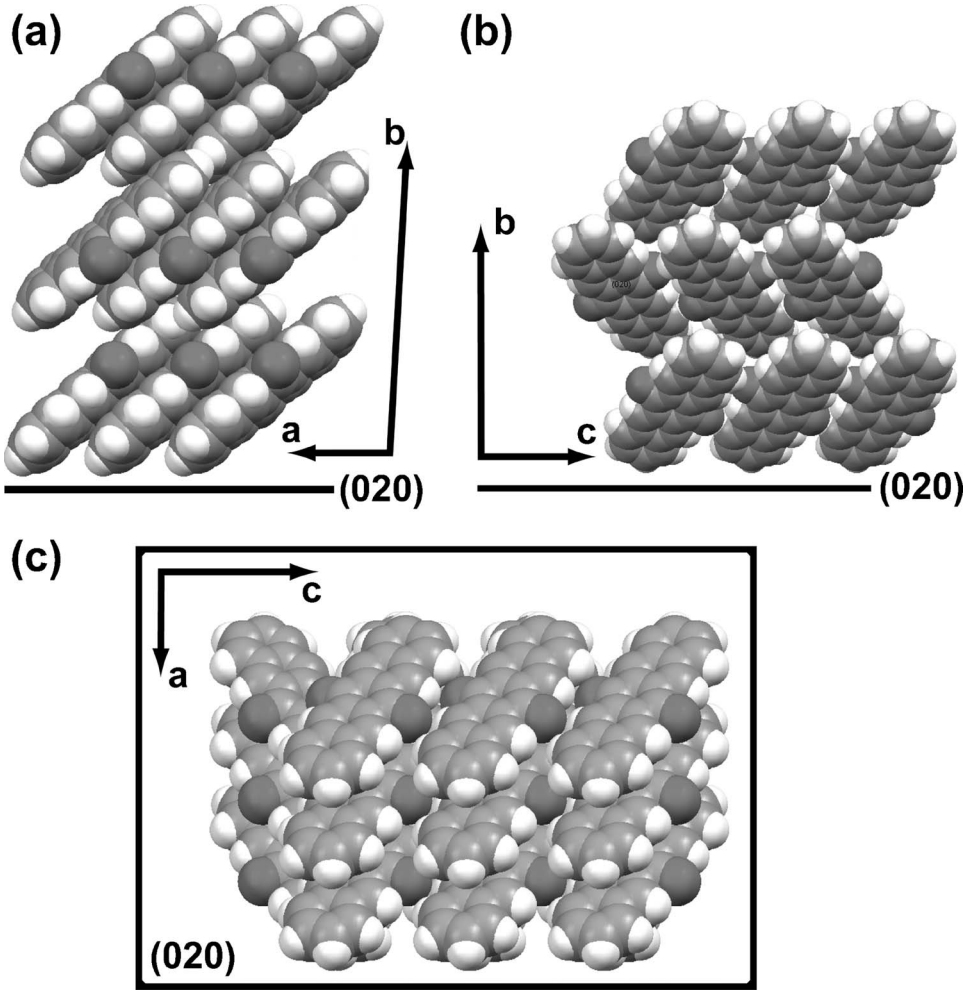


FIG. 8. The bulk structure of PQ viewed in projection on (a) the *ab* plane, (b) the *bc* plane, and (c) the *ac* plane of the unit cell together with the position of the (020) net plane that was found as most intense reflection within XRD (Fig. 7), visualization performed by MERCURY (Ref. 46).

spective bulk phases of P and PQ). The spectra presented in Figs. 10(a) and 10(b) of P show a significant shift of all absorptions compared to the bulk reference, which agrees with our finding of preferential growth in the P thin-film polymorph. Compared to the P contributions in the spectra of sample P+PQ, the peak positions remain essentially unchanged (shifts $\leqslant 1$ cm$^{-1}$), which agrees with our results from x-ray diffraction, where we found exclusively the P thin-film phase. This also corroborates our proposition of pronounced phase separation within codeposited films of P and PQ, since IR spectroscopy is highly sensitive to a potential intercalation of P and PQ. For PQ, we observe rather the opposite behavior, i.e., the spectrum of the pure film matches well the reference (dominating bulk phase, as found in XRD), whereas certain PQ peaks in the spectrum of P+PQ are significantly shifted (dominating PQ thin-film phase, shifts of up to 5 cm$^{-1}$). PQ peaks of the pure sample that show a shift of maximum of 1 cm$^{-1}$ compared to the reference are heavily shifted (up to 5 cm$^{-1}$) in the codeposited film (preferred thin-film phase). Particularly, in the region of CH out-of-plane bending and stretching modes,[54,55] the influence of the different molecular orientations within the polymorphs is apparent [P: 729(+1), 904(+1), and 954(±0) cm$^{-1}$; PQ: 763(−5), 933(+5), 958(±0), and 988 (+2) cm$^{-1}$, shifts of pure materials relative to P+PQ in brackets]. This also holds for the region of other vibrations of outer atoms like the CO bond vibrations[15,56,57] of PQ [1674(+3)], whereas the frequencies of carbon backbone vibrations like CC ring stretch modes[58] [P: 1296(±0) and 1344(±0); PQ: 1190(±0) and 1396(±0)] remain unchanged. The CC stretch modes of the reference data in the region 1440–1540 cm$^{-1}$ along the molecular axis of P are suppressed due to the almost perpendicular orientation of P molecules on $SiO_2$ within the thin-film phase,[54,59] whereas this is not true for PQ in the pure and codeposited film [1443(+1), 1453(±0), 1574(−1), and 1584(−1) cm$^{-1}$], since the molecules have a higher inclination within the PQ thin-film phase.

Finally, we investigated the optical properties of pure and codeposited films of P and PQ on quartz by means of visible-UV absorption spectroscopy in normal transmission geometry (Fig. 11). We found the onset of the lowest-energy transition, attributed to the P energy gap, at 1.79 eV with its peak maximum at 1.85 and 1.94 eV (the two components of the Davydov 0-0 band doublet[60]), as well as the the 0-1 band (at 2.12 and 2.28 eV, respectively). This result is in good agreement with previously reported results for P thin films on oriented poly(tetrafluoroethylene),[61] $Al_2O_3$ (sapphire),[62] and quartz.[60,63] For the pure PQ film on quartz the first peak maximum, assigned to the fundamental absorption, appears at 2.92 eV (low-energy onset at 2.81 eV) and at 3.09 eV, respectively, which is in good agreement with the results

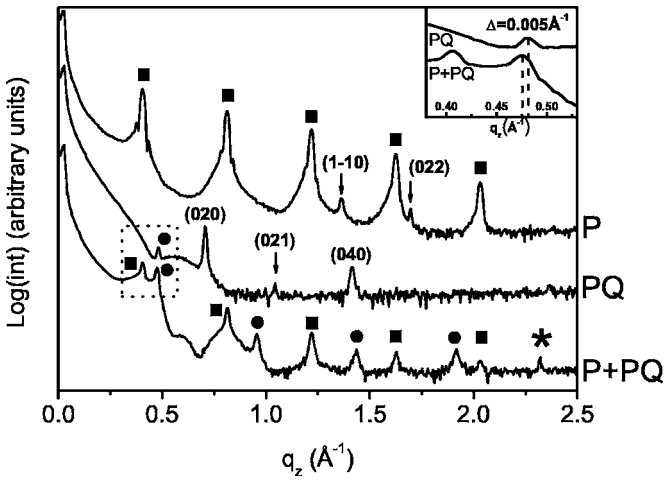


FIG. 9. X-ray-diffraction scans of samples P, PQ, and P+PQ. Reflections of the bulk phases are indicated with the respective Miller indices, and peaks originating from the thin-film phase (001) series are indicated with a square (P) and a circle (PQ), respectively. The star in spectrum P+PQ marks a parasitic second-order reflection of the silicon (004) plane. The inset shows a zoomed representation of the dotted area around the PQ (001) thin-film phase reflection that shows a shift $\Delta$ of 0.005 $\text{Å}^{-1}$ within the P+PQ sample if compared to the pure PQ film.

found for PQ on sapphire.[41] The absorption spectrum of the codeposited sample is almost a simple superposition of the individual spectra of the pure materials. The first four peaks at lower energies in the spectrum of P+PQ exhibit no significant shift compared to pure P. In contrast, the two absorption features corresponding to the fundamental absorptions of PQ exhibit a shift of 0.1 eV compared to the spectrum of pure PQ. This finding suggests that the growth of P, PQ, and P+PQ on quartz follows the same trends as observed for $SiO_2$ substrates. That is, the presence of P during codeposition induces a PQ growth in a different polymorph.

## VI. SUMMARY AND OUTLOOK

Using a number of experimental techniques, we found evidence of pronounced phase separation in codeposited thin films of pentacene and pentacenequinone. Pure films PQ (Fig. 7) exhibit polymorphic growth on $SiO_2$ in the thin film and bulk phase. If sequentially deposited, both materials preferentially grow on top of each other. We found that the presence of P (as underlayer in sequential deposition or if codeposited) induces PQ growth preferentially in the thin-film phase. The ratio between PQ bulk and thin-film phases was found to be sensitive to $\kappa$ (more thin-film phase at increased $\kappa$). For codeposited films of $\chi$=30 nm, no PQ bulk phase contributions could be found via XRD, although apparent in AFM and SEM images. This indicates nontextured growth of the PQ bulk phase needlelike crystallites on $SiO_2$. The lattice spacing $d_{001}$ of the P thin-film polymorph was insensitive to the presence of PQ, whereas $d_{001}$ of the PQ thin-film phase is increased by 0.013 nm in case of codeposition, indicating a more upright orientation of the molecules. We showed that the island density also in codeposited films depends on the deposition rate $\kappa$. Therefore, $\kappa$ was identified as key parameter to control the length scale of phase separation obtained by codeposition in this system. Moreover,

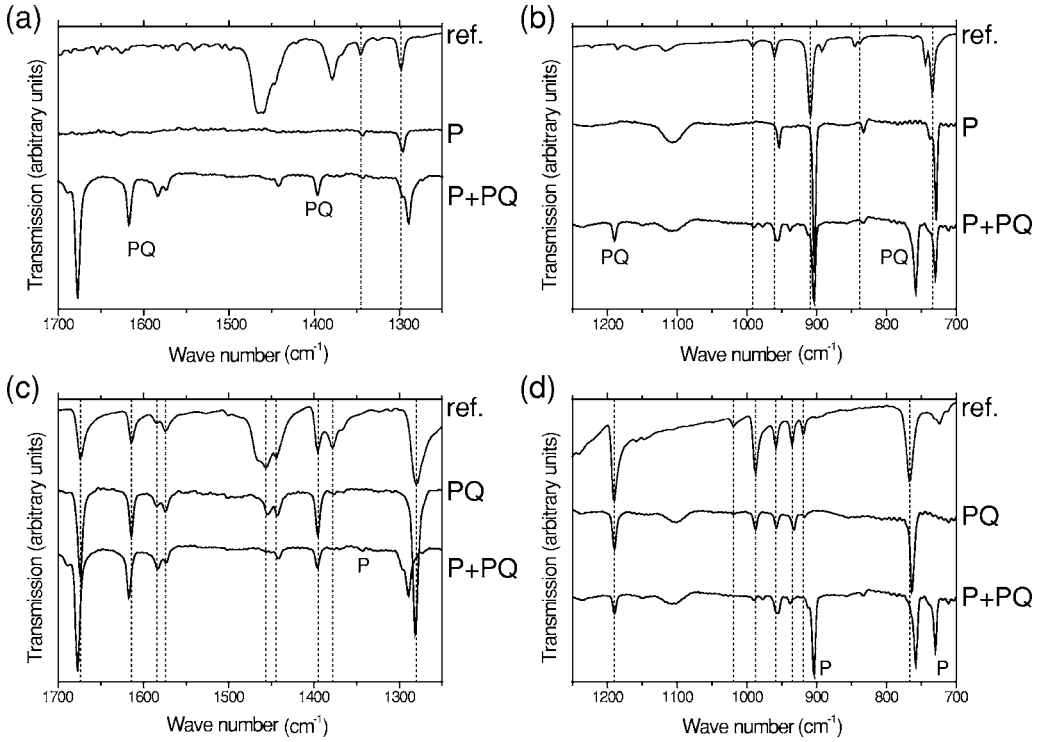


FIG. 10. FTIR spectra of samples [(a) and (b)] P and [(c) and (d)] PQ compared to sample P+PQ and a KBr reference spectrum provided by the manufacturer. Peaks originating from the second compound within the spectrum of P+PQ are marked as P and PQ, respectively.

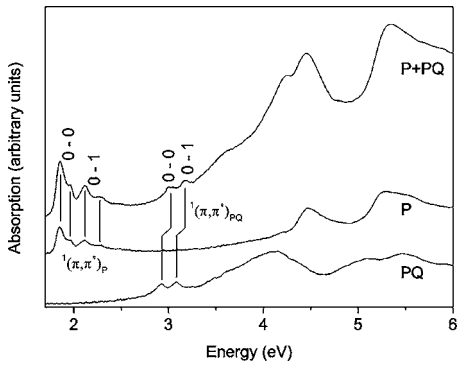


FIG. 11. Visible-UV absorption spectra of P, PQ ($\chi$=30 nm), and 1:1 co-deposited P+PQ films (total $\chi$=30 nm) on quartz. The curves are vertically shifted for better visibility.

FTIR spectroscopy showed that no significant intercalation of P and PQ molecules takes place during growth. The high degree of crystallinity we found in both pure and codeposited films and the pronounced phase separation meet the requirements of bulk heterojunction materials for photovoltaic applications. As device structure, we tested a coevaporated film of P+PQ sandwiched between poly(3,4-ethylenedioxythiophene):poly(styrenesulfonate) coated indium tin oxide as transparent high work function ($\phi$) electrode ($\phi \approx 5.1$ eV) (Ref. 64) and samarium ($\phi \approx 2.7$ eV) (Ref. 22) as low work function electrode. These preliminary experiments did not yield reproducible current-voltage characteristics, most likely due to the highly corrugated surface of P+PQ films (Fig. 6). Further experiments are in progress to address this issue via the variation of the molar ratio and the modification of preparation parameters in order to improve the applicability of P+PQ heterostructures.

## ACKNOWLEDGMENTS

We thank Roland Resel and Martin Oehzelt (both at Graz University of Technology, Austria) for preliminary XRD measurements, Piero Cosseddu (University of Cagliari, Italy) for supporting AFM work, as well as Jens Pflaum (Universität Stuttgart, Germany) for fruitful discussions. This work was supported by the Sfb448 (DFG). R.O. is supported by the "Berliner Programm zur Förderung der Chancengleichheit für Frauen in Forschung und Lehre." N.K. acknowledges financial support by the Emmy Noether-Program (DFG).

*Electronic address: norbert.koch@physik.hu-berlin.de

[1] R. Wisnieff, Nature (London) **394**, 225 (1998).
[2] N. Koch, A. Vollmer, I. Salzmann, B. Nickel, H. Weiss, and J. P. Rabe, Phys. Rev. Lett. **96**, 156803 (2006).
[3] G. Horowitz, Adv. Mater. (Weinheim, Ger.) **10**, 365 (1998).
[4] C. D. Dimitrakopoulos, S. Purushothaman, J. Kymissis, A. Callegari, and J. M. Shaw, Science **283**, 822 (1999).
[5] C. Dimitrakopoulos and P. Malenfant, Adv. Mater. (Weinheim, Ger.) **14**, 99 (2002).
[6] M. Halik, H. Klauk, U. Zschieschang, G. Schmid, S. Ponomarenko, S. Kirchmeyer, and W. Weber, Adv. Mater. (Weinheim, Ger.) **15**, 917 (2003).
[7] Y.-Y. Lin, D. Gundlach, S. Nelson, and T. Jackson, IEEE Electron Device Lett. **18**, 606 (1997).
[8] P. F. Baude, D. A. Ender, M. A. Haase, T. W. Kelley, D. V. Muyres, and S. D. Theiss, Appl. Phys. Lett. **82**, 3964 (2003).
[9] S. Lee, B. Koo, J. Shin, E. Lee, H. Park, and H. Kim, Appl. Phys. Lett. **88**, 162109 (2006).
[10] Y. Kato, S. Iba, R. Teramoto, T. Sekitani, T. Someya, H. Kawaguchi, and T. Sakurai, Appl. Phys. Lett. **84**, 3789 (2004).
[11] M. Shtein, J. Mapel, J. B. Benziger, and S. R. Forrest, Appl. Phys. Lett. **81**, 268 (2002).
[12] F. Garnier, Chem. Phys. **227**, 253 (1998).
[13] T. Minari, T. Nemoto, and S. Isoda, J. Appl. Phys. **96**, 769 (2004).
[14] T. Minakata, H. Imai, M. Ozaki, and K. Saco, J. Appl. Phys. **72**, 5220 (1992).
[15] O. D. Jurchescu, J. Baas, and T. T. M. Palstra, Appl. Phys. Lett. **84**, 3061 (2004).
[16] N. Koch, I. Salzmann, R. L. Johnson, J. Pflaum, R. Friedlein, and J. P. Rabe, Org. Electron. **7**, 537 (2007).
[17] T. B. Singh, P. Senkarabacak, N. S. Sariciftci, A. Tanda, C. Lackner, R. Hagelauer, and G. Horowitz, Appl. Phys. Lett. **89**, 033512 (2006).
[18] T. Singh, F. Meghdadi, S. Gnes, N. Marjanovic, G. Horowitz, P. Lang, and N. Bauer, S. Sariciftci, Adv. Mater. (Weinheim, Ger.) **17**, 2315 (2005).
[19] M. Ahles, R. Schmechel, and H. von Seggern, Appl. Phys. Lett. **87**, 113505 (2005).
[20] T. Yasuda, T. Goto, K. Fujita, and T. Tsutsui, Appl. Phys. Lett. **85**, 2098 (2004).
[21] J. H. Kang, D. da Silva Filho, J.-L. Bredas, and X.-Y. Zhu, Appl. Phys. Lett. **86**, 152115 (2005).
[22] N. Koch, J. Ghijsen, R. L. Johnson, J. Schwartz, J.-J. Pireaux, and A. Kahn, J. Phys. Chem. B **106**, 4192 (2002).
[23] G. Yu, J. Gao, J. C. Hummelen, F. Wudl, and A. J. Heeger, Science **270**, 1789 (1995).
[24] J. Nelson, Science **293**, 1059 (2001).
[25] J. Nelson, Curr. Opin. Solid State Mater. Sci. **6**, 87 (2002).
[26] P. Peumans, A. Yakimov, and S. R. Forrest, J. Appl. Phys. **93**, 3693 (2003).
[27] B. Brousse, B. Ratier, and A. Moliton, Thin Solid Films **451-452**, 8185 (2004).
[28] I. P. M. Bouchoms, W. A. Schoonveld, J. Vrijmoeth, and T. M. Klapwijk, Synth. Met. **104**, 175 (1999).
[29] D. J. Gundlach, T. N. Jackson, D. G. Schlom, and S. F. Nelson, Appl. Phys. Lett. **74**, 3302 (1999).
[30] C. C. Mattheus, A. B. Dros, J. Baas, G. T. Oostergetel, A. Meetsma, J. L. de Boer, and T. M. Palstra, Synth. Met. **138**, 475 (2003).
[31] M. Oehzelt, R. Resel, C. Suess, R. Friedlein, and W. R. Salaneck, J. Chem. Phys. **124**, 054711 (2006).
[32] S. Fritz, S. Martin, C. Frisbie, M. Ward, and M. Toney, J. Am. Chem. Soc. **126**, 4084 (2004).

[33] A. V. Dzyabchenko, V. E. Zavodnik, and V. K. Belsky, Acta Crystallogr., Sect. B: Struct. Crystallogr. Cryst. Chem. **35**, 2250 (1979).
[34] F.-J. Meyer zu Heringdorf, M. C. Reuter, and R. M. Tromp, Nature (London) **412**, 517 (2001).
[35] R. Ruiz, D. Choudhary, B. Nickel, T. Toccoli, K.-C. Chang, A. Mayer, P. Clancy, J. Blakely, R. Headrick, S. Iannotta *et al.*, Chem. Mater. **16**, 4497 (2004).
[36] R. Ruiz, A. C. Mayer, G. G. Malliaras, B. Nickel, G. Scoles, A. Kazimirov, H. Kim, R. L. Headrick, and Z. Islam, Appl. Phys. Lett. **85**, 4926 (2004).
[37] A. C. Mayer, R. Ruiz, R. L. Headrick, A. Kazimirov, and G. G. Malliaras, Org. Electron. **5**, 257 (2004).
[38] R. Ruiz, B. Nickel, N. Koch, L. C. Feldman, R. F. Haglund, A. Kahn, and G. Scoles, Phys. Rev. B **67**, 125406 (2003).
[39] R. Ruiz, B. Nickel, N. Koch, L. C. Feldman, R. F. Haglund, A. Kahn, F. Family, and G. Scoles, Phys. Rev. Lett. **91**, 136102 (2003).
[40] S. D. Wang, X. Dong, C. S. Lee, and S. T. Lee, J. Phys. Chem. B **109**, 9892 (2005).
[41] D. Hwang, K. Kim, J. Kim, D.-Y. Jung, E. Kim, and S. Im, Appl. Surf. Sci. **244**, 615 (2005).
[42] C. D. Dimitrakopoulos, A. R. Brown, and A. Pomp, J. Appl. Phys. **80**, 2501 (1996).
[43] C. Mattheus, G. de Wijs, R. de Groot, and T. Palstra, J. Am. Chem. Soc. **125**, 6323 (2003).
[44] S. Pratontep, M. Brinkmann, F. Nuesch, and L. Zuppiroli, Phys. Rev. B **69**, 165201 (2004).
[45] H. Klauk and T. Jackson, Solid State Technol. **43**, 63 (2000).
[46] C. F. Macrae, P. R. Edgington, P. McCabe, E. Pidcock, G. P. Shields, R. Taylor, M. Towler, and J. van de Streek, J. Appl. Crystallogr. **39**, 453 (2006).
[47] W. Kraus and G. Nolzeb, J. Appl. Crystallogr. **29**, 301 (1996).
[48] P. Scherrer, Nachr. Ges. Wiss. Goettingen, Math.-Phys. Kl. **2**, 98 (1918).
[49] J. I. Langford and A. J. C. Wilson, J. Appl. Crystallogr. **11**, 102 (1978).
[50] T. L. Threlfall, Analyst (Cambridge, U.K.) **120**, 2435 (1995).
[51] J. H. Sharp and M. Abkowitz, J. Phys. Chem. **77**, 477 (1973).
[52] A. Napier and R. A. Collins, Thin Solid Films **248**, 166 (1994).
[53] M. M. El-Nahass, K. F. Abd-El-Rahman, and A. A. A. Darwish, Mater. Chem. Phys. **92**, 185 (2005).
[54] J. Szczepanski, C. Wehlburg, and M. Vala, Chem. Phys. Lett. **232**, 221 (1995).
[55] D. M. Hudgins and S. A. Sandford, J. Phys. Chem. A **102**, 344 (1998).
[56] M. Avram and G. D. Mateescu, *Infrared Spectroscopy* (Wiley, New York, 1972).
[57] D. Hadži and N. Sheppard, J. Am. Chem. Soc. **73**, 5460 (1951).
[58] S. R. Langhoff, J. Phys. Chem. **100**, 2819 (1996).
[59] Y. Hosoia, K. Okamuraa, Y. Kimuraa, H. Ishiia, and M. Niwanoa, Appl. Surf. Sci. **244**, 607 (2005).
[60] Q. Miao, T.-Q. Nguyen, T. Someya, G. Blanchet, and C. Nuckolls, J. Am. Chem. Soc. **125**, 10284 (2003).
[61] M. Brinkmann, S. Graff, C. Straupe, J.-C. Wittmann, C. Chaumont, F. Nuesch, A. Aziz, M. Schaer, and L. Zuppiroli, J. Phys. Chem. B **107**, 10531 (2003).
[62] K. Kim, Y. K. Yoon, M.-O. Mun, S. P. Park, S. S. Kim, S. Im, and J. H. Kim, J. Supercond. **15**, 595 (2002).
[63] R. He, N. G. Tassi, G. B. Blanchet, and A. Pinczuk, Appl. Phys. Lett. **87**, 103107 (2005).
[64] N. Koch, A. Elschner, J. Rabe, and R. Johnson, Adv. Mater. (Weinheim, Ger.) **17**, 330 (2005).
[65] The height information obtained from AFM was assumed to be more reliable in case of intrinsic steps as in the case of steps between P and $SiO_2$ due to the different mechanical properties of the materials in the latter case (intrinsic P steps of multilayer films, however, exhibit a mean step height of 1.6 nm).